Design and Performance Evaluation of Triangular Microstrip Patch Array Antennas for Cyber-Physical System Applications

Masuk Abdullah
Department of Vehicle Engineering, University of Debrecen, Otemeto strt. 2-4, 4028 Debrecen, Hungary
masuk@eng.unideb.hu (corresponding author)

Received: 18 April 2025 | Revised: 16 May 2025 | Accepted: 25 May 2025

 DOI: https://doi.org/10.48084/etasr.11584

ABSTRACT

This study presents the design and performance evaluation of Triangular Microstrip Patch Array (TMPA) antennas for Cyber Physical System (CPS) applications. In response to the growing demand for sophisticated multiband antennas in CPSs, TMPAs implemented on Printed Circuit Boards (PCBs) offer a cost-effective and high-performance solution. The study focuses on the fabrication and assessment of copper-based TMPAs operating at L-band (1.3 GHz) and S-band (3.1 GHz) frequencies, optimized for gain and impedance matching. The experimental results show that the L-band TMPA achieved a gain of 14.80 dBi, closely matching the reference antenna's 14.46 dBi. The S-band TMPA reached a gain of 15.47 dBi, within 0.3 dBi of the reference. The near-field measurements confirmed a minimal phase variation, although slight polarization notches were observed. These results demonstrate the suitability of TMPAs for CPS applications, particularly in phased array configurations, where reliable beamforming and minimal signal loss are critical. Future work will focus on enhancing automated testing facilities to further improve antenna performance evaluation in CPS environments.

Keywords-antenna design; antenna performance; patch array antenna; CPS

I. INTRODUCTION

CPSs have an impact on society, the economy, and people's daily lives; hence, industry 4.0, government, and academic research have focused on this system. The former are innovative tools that advanced industries can use to create new frequency-band sensors and communication systems [1]. Industrial remote services demonstrate CPS potential and sensor communication demands. CPS modeling subjects include electric vehicles and mechatronics system engineering [2]. The CPS idea is projected to remain high owing to the enhanced radar sensor technology and new domains, such as CPS implementation in the cost-effective construction of Microstrip Patch Antennas (MPAs) [3-5]. The concept of the microstrip antenna was introduced in 1953 [6, 7], but it took approximately two decades to be realized following the advancements in the printed circuit board technology [8, 9]. Since then, MPAs have been the most popular type of antenna. They are lightweight, inexpensive, compact in design, and easy to conform. They also have a geometrical configuration, superior portability, suitability for arrays, easy fabrication, and easy integration with sensors. A conducting patch of any planar or nonplanar shape can be used to create an MPA. This patch is placed on one side of the dielectric substrate, and the opposite side of the substrate is a ground plane. It is a printed resonant antenna widely applied in microwave wireless communication networks.

The selection of chemical copper (Cu) in the FR4 substrate as a substrate of this antenna was based on the premise that a successful antenna design on copper can lead to the development of an interesting low cost conformal and planar future microstrip design, including the optically transparent MPA. FR4 is a common material for PCBs, with copper foil laminated to one or both sides, known as copper clad laminates, with varying thickness or weights [10, 11]. Figure 1 shows a schematic layout of the Cu and conducting polymer patches in the TMP antenna.

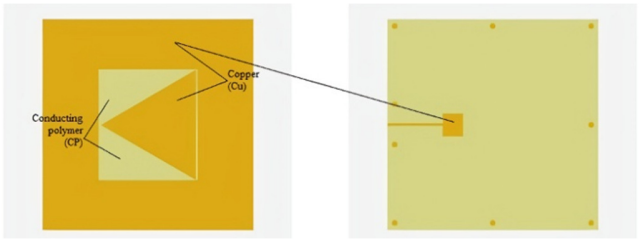

Fig. 1. Schematic layout of Cu and CP in the designed TMP single element antenna.

Cu is approximately twice as conductive as aluminum (Al) and six times more conductive than steel, making it an excellent material choice for antenna design. Among the materials evaluated, antennas using copper for both the patch and ground plane exhibited the lowest return loss, measured at 41.84 dB at a resonant frequency of 8.55 GHz. In contrast,

stainless steel, which has the lowest conductivity among the tested materials, resulted in the highest bandwidth, providing 0.656 GHz [12]. The integration of antennas into PCBs has become common in CPS applications, as the PCB technology enables compact, low-cost, and reliable configurations. Due to their favorable characteristics, TMP antennas are widely used in aerospace systems, such as satellites, missiles, and aircraft.

II. TMP ANTENNA DESIGN, SIMULATION, AND FABRICATION

A. Modeling and Design Aspects

The design process began with a three-layer PCB-based TMP antenna configured with two channels, operating at L-band (1.3 GHz) and S-band (3.1 GHz) frequencies. The TMP antenna was developed to support both horizontal and vertical array configurations. Figure 2 presents the design process flowchart for the proposed TMP array antenna, including the feed channels and the corresponding array elements.

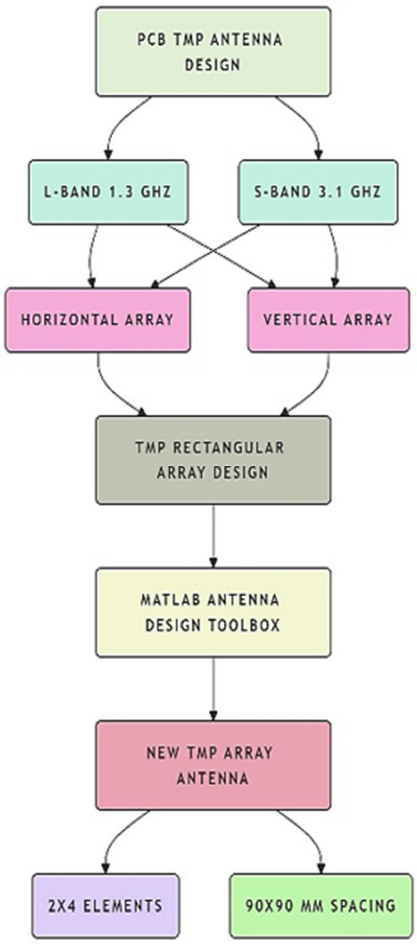

Fig. 2. Proposed design process flowchart of the TMP array antenna.

In CPS environments, phased-array designs involving various PCB antenna types are commonly implemented. Figure 3 illustrates the fundamental layout of the proposed TMP triangular array antenna.

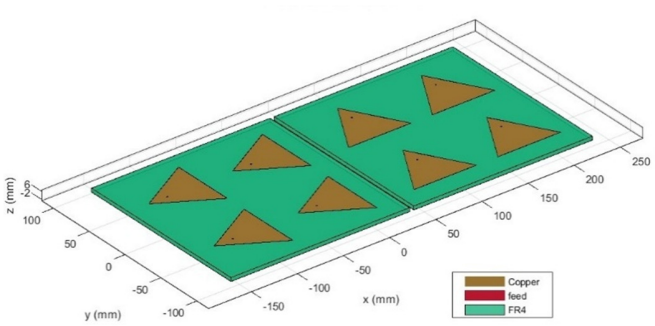

Fig. 3. Fundamental design of the TMP array antenna.

The TMP array antenna, comprising 2 × 4 elements with 90 × 90 mm spacing, was designed using the MATLAB Design Toolbox and other relevant software. Figure 4 presents both the horizontal and vertical configurations of the TMP array antenna within the PCB layout.

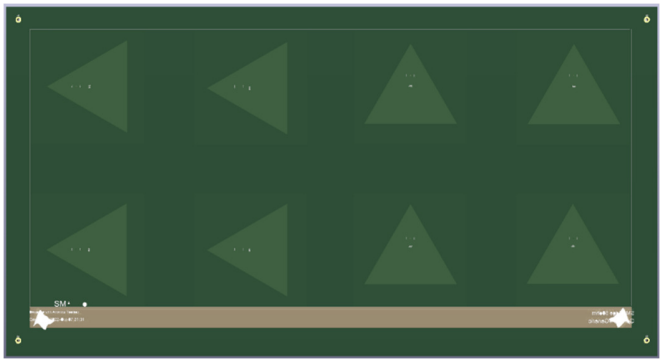

Fig. 4. PCB antenna design with (2 × 4 elements) for the TMP array antenna.

B. Simulation and Perfomace

Key antenna characteristics, such as the gain, half-power beamwidth (−3 dB), and sidelobe level, were optimized through simulation, with a focus on mechatronics engineering applications. This approach minimizes potential design errors. In a phased-array configuration, antenna elements (radiators) are fed with varying phase shifts, enabling electronic beam steering using a unified design. Electrical steering offers greater flexibility and lower maintenance requirements compared to mechanical steering.

At zero wavenumber *(k=0)* and an azimuth angle *θ=90°*, the normalized power gain *(G)* of the phased-array antenna is given by [13]:

$$G(\theta) = \left| \frac{\sin\left(\frac{Nkd}{2}\right)\cos\theta}{N\sin\left(\frac{kd}{2}\right)\cos\theta} \right|^2 \quad (1)$$

where *N* represents the elements and d is the element distance. With the given value, the length of a can be calculated for $f_r =$ 3.1 GHz and 1.3 GHz as the center frequency, $c = 3 \times 10^8$ m/s and $\varepsilon_r = 4.8$

To determine the side length L of the Triangular Patch Antenna (TPA), the patch is modeled as an equilateral triangle with equal sides and internal angles. Using (1) and the known parameters, the corresponding length can be calculated. According to [14], the resonant frequency f_r of an equilateral triangular patch is given by:

$$f_r = \frac{c}{2L\sqrt{\varepsilon_r}} \quad (2)$$

where c is the speed of light in a vacuum, L is the side length of the equilateral triangle, and ε_r is the relative permittivity (dielectric constant) of the substrate.

Finally, the side length of the triangular patch was calculated as L=67.695 mm. Accordingly, the corresponding height *(H)* of the equilateral triangle was determined using:

$$H = \sqrt{L^2 - (\frac{1}{2} \times L)^2} \quad (3)$$

The 3D radiation pattern shown in Figure 5 illustrates the performance of the S-band TMP array antenna with a 2 × 4 element configuration.

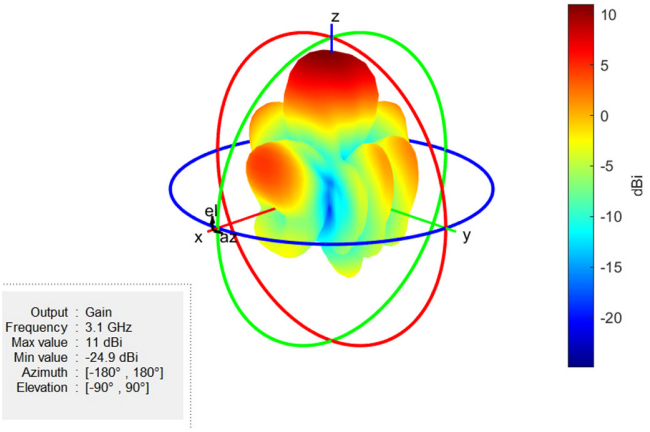

Fig. 5. 3D radiation pattern of the S-band TMP array antenna (2×4 elements).

The impedance of the microstrip PCB antenna reflects the characteristic impedance of the microstrip transmission line. To minimize the signal reflections, this impedance is standardized by adjusting the cross-sectional dimensions of the microstrip, as described in (2).

To ensure optimal impedance matching during the patch antenna measurements, the input impedance must be as close as possible to 50 Ω. The input impedance of the transmission line can be calculated as:

$$Z_{in} = Z_0 \frac{Z_L + jZ_0 \tan \beta L}{Z_0 + jZ_L \tan \beta L} \quad (4)$$

where L is the transmission line length, Z_L is the load impedance (Ω), and Z_{in} is the input impedance of the transmission line (Ω) and:

$$\beta = \frac{2\pi}{\lambda} \quad (5)$$

where λ corresponds to the wavelength.

To ensure a maximum power transfer from the Radio Frequency (RF) circuitry to the antenna with a minimal signal reflection, the antenna's input impedance must be properly matched to 50 Ω.

The Standing Wave Ratio (SWR) is a key parameter that indicates how effectively power is transmitted through a transmission line. Efficient impedance matching is essential to minimize reflections, with engineers devoting a significant effort to achieving optimal matching conditions [15, 16]:

$$SWR = \frac{1+|r|}{1-|r|} \quad (6)$$

where r is the reflection coefficient, calculated as:

$$r = \frac{Z_L - Z_0}{Z_L + Z_0} \quad (7)$$

Impedance matching is the process of adjusting or coupling the antenna's input impedance Z_L to the output impedance of the RF circuitry Z_0, which is typically 50 Ω. According to (7), a perfect match is achieved when Z_L=Z_0.

C. Fabrication Proceduce

The S-band (3.1 GHz) antenna was fabricated by an external manufacturer, while the L-band (1.3 GHz) antenna was produced in-house at the Mechatronics Engineering Laboratory of the University of Debrecen. Milling and drilling machines were used to fabricate the L-band TMP array antenna directly onto PCB substrates. This method offers precision, adaptability, and ease of use. Operating at 40,000 RPM, the PCB plotter removes copper from the base material without the need for chemical etching. The triangular microstrip patch antenna was fabricated using an LPKF ProtoMat S104, following the analysis of the KiCad manufacturing files. Although this technique supports clean, chemical-free prototyping, it can be combined with etching to reduce the tool wear and operating costs. Etching involves selectively removing excess copper using a chemical solution, leaving only the intended circuit pattern. Figure 6 shows an example of PCB printing via chemical processing.

The mixture contained hydrogen peroxide (H_2O_2) and hydrochloric acid (HCl), which then reacted with copper metal to produce copper chloride and water:

$$H_2O_2 + C_u(s) + 2HCl(aq) \longrightarrow C_uCl_2 + 2H_2O \quad (8)$$

This process is classified as a redox (reduction–oxidation) reaction:

$$Oxidation\ reaction\ Cu^0 - 2e^- \longrightarrow Cu^{II} \quad (9)$$

$$Reduction\ reaction\ 2O^{-I} + 2e^- \longrightarrow 2O^{-II} \quad (10)$$

Hydrogen peroxide (H_2O_2) acts as the oxidizing agent, while copper (Cu) serves as the reducing agent.

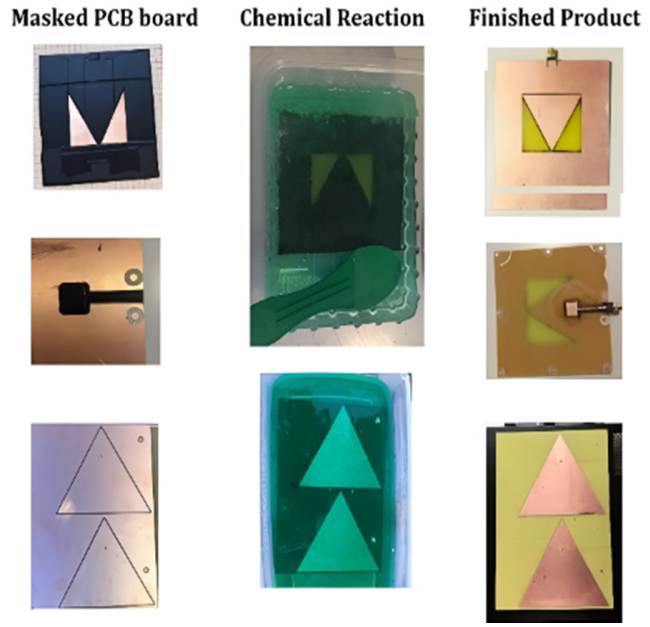

Fig. 6. PCB printing via chemical reactions.

Figure 7 presents various fabricated TMP array antennas with different element configurations.

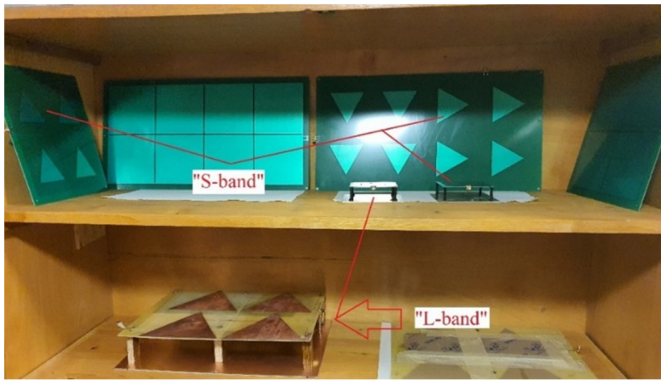

Fig. 7. Different types of TMP array antennas with specific element configurations.

III. TEST SETUP AND MEASUREMENT RESULTS

The test environment included calibration procedures and relevant antenna parameters, alongside the in-situ setup, measurement results, and observed differences between the theoretical and fabricated antenna performance. Near-field measurements are inherently more complex, as both amplitude and phase information must be captured with high correlation to the reference signal source. The evaluation also includes near-field to far-field transformation coefficients.

Far-field radiated emission measurements are required globally to ensure compliance with the regulatory standards. Meanwhile, in situ measurements conducted at a 2.6 m distance are used to assess mutual antenna interference, radiation patterns, and near-field characteristics. These measurements also support the evaluation of product prototypes, individual modules, and design modifications prior to commercialization. The CPS Laboratory's near-field measurement facility, known as the in situ range, was used for testing. The antenna setup is depicted in Figure 8.

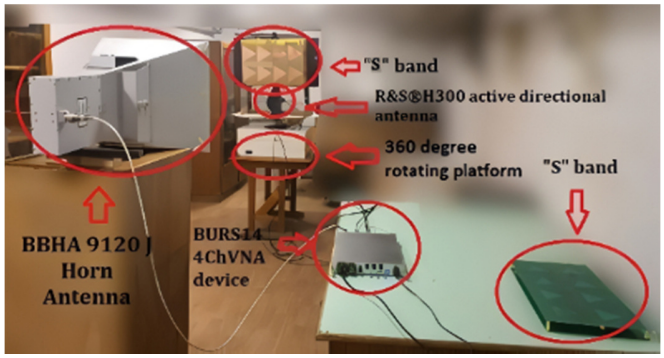

Fig. 8. Test setup environment for antenna measurement.

Figure 8 illustrates the complete experimental setup used for near-field antenna measurements. The measurement system was built around a computer controlled four Channel Vector Network Analyzer (4ChVNA), which included one RF signal transmitter and four synchronized receivers. The system supported simultaneous acquisition of signals from multiple antenna ports, enabling a comprehensive characterization of the array performance. Both L-band (1.3 GHz) and S-band (3.1 GHz) antennas were connected to the setup, with each frequency band corresponding to a distinct measurement channel.

The Antenna Under Test (AUT) was mounted on a precision-controlled 360° rotating platform, allowing for full azimuthal scanning and accurate pattern acquisition. As the excitation source, a BBHA 9120 J horn antenna transmitted a calibrated, linearly polarized signal across the designated frequency band. For reference purposes, an R&S® H300 active directional antenna was used to benchmark the performance of the rotating AUT. To ensure polarization alignment and signal fidelity, linear cross-polarization was employed throughout the measurements. The 4ChVNA (model BURS14) captured the signal responses from the antenna under testing. The system was interfaced with a PC via LAN connection, which allowed real-time control, data acquisition, and signal processing. The entire process was automated and managed through custom software that synchronized the rotation steps with signal capture, ensuring repeatable and high-resolution radiation pattern measurements.The fabricated TMP array antenna was evaluated under controlled near-field conditions within the CPS Laboratory's in -situ test range. Following the experimental procedures, appropriate electromagnetic formulations were applied to transform the measured near-field data into far-field quantities. This enabled the precise calculation of key antenna parameters, such as maximum gain, beam direction, and sidelobe levels. In particular, the gain at the L-band center frequency of 1.3 GHz was determined in dBi through calibrated measurements. The resulting radiation pattern of the L-band TM array antenna referenced to the azimuthal direction is shown in Figure 9.

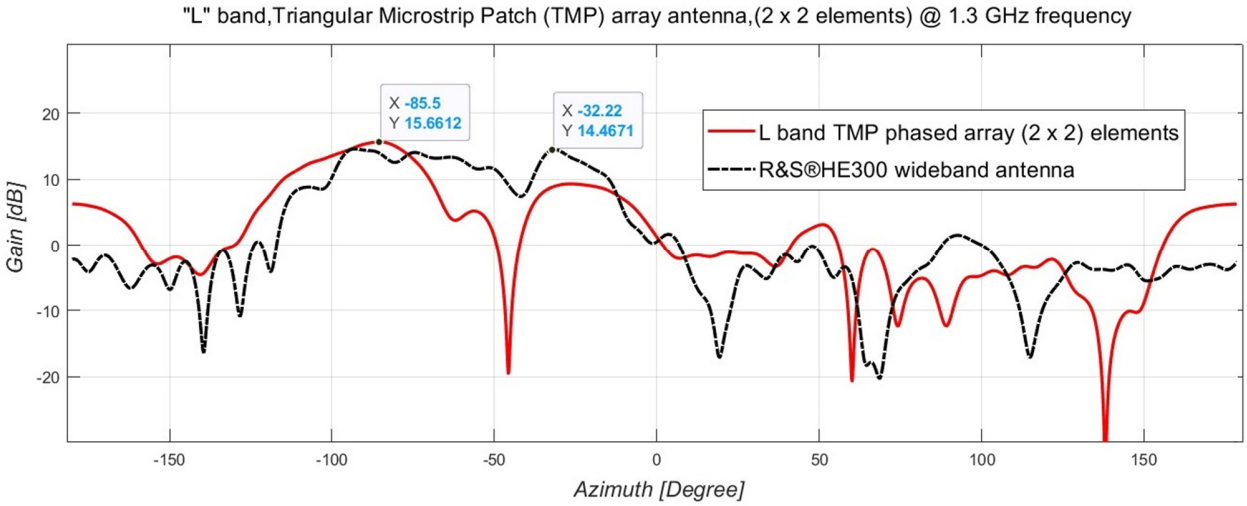

Fig. 9. Measured TMP array radiation pattern at 1.3 GHz (L-band).

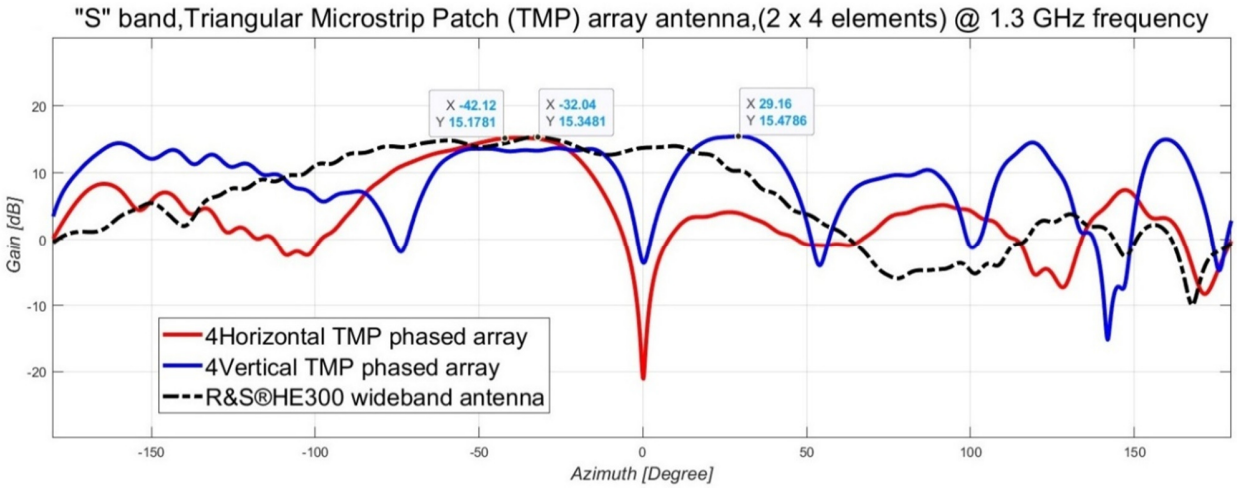

Fig. 10. Measured TMP array radiation pattern at 1.3 GHz (S-band).

Figure 9 displays the measured gain of the L-band TMP array with four vertical elements, which reached 15.66 dBi. In comparison, the R&S® H300 reference antenna achieved a gain of 14.46 dBi under the same conditions. Figure 10 presents the radiation pattern of the S-band TMP array, which was also tested at 1.3 GHz for comparison purposes.

The gain difference between the fabricated antennas and the reference remains within 1 dBi, indicating strong performance consistency. However, small notches appear in the measured patterns due to slight phase shifts caused by polarization drift, likely related to minor alignment issues during testing.

According to Figure 10, the measured gain was 15.17 dBi for the vertical array and 15.47 dBi for the horizontal array, while the R&S® H300 reference antenna measured at 15.34 dBi. The black dotted lines in Figures 9 and 10 represent the reference antenna's radiation pattern for comparison.

In both cases, the gain difference between the fabricated and reference antennas stays within 0.3 dBi, confirming the effectiveness of the TMP array design. However, slight notches appear in the radiation patterns due to phase shifts caused by a polarization drift. These effects are likely related to measurement alignment or fabrication tolerances.

Such results support the suitability of TMP array antennas for integration into CPS applications, where both single-element and phased-array configurations are essential for advanced sensing and communication tasks.

IV. CONCLUSION

This study presented the design, fabrication, and performance evaluation of Triangular Microstrip Patch Array (TMPA) antennas for Cyber Physical System (CPS) applications. Copper-based TMPAs demonstrated gains comparable to those of the reference antennas, with minimal phase variation and alignment within 1 dBi in the L-band

(1.3 GHz) and within 0.3 dB in the S-band (3.1 GHz). These results confirm the effectiveness of the design in phased-array configurations, where accurate beam steering and impedance matching are critical for CPS integration.

The antennas were optimized for dual-band operation and implemented using low-cost PCB fabrication techniques. Compared with prior designs [1–5], the proposed TMPAs achieved an improved gain (up to 15.47 dBi), consistent impedance matching, and practical manufacturability, rendering them a strong candidate for scalable phased-array CPS deployments.

To further improve the measurement accuracy, the CPS laboratory setup could benefit from automated antenna rotation and enhanced shielding against reflections, multipath interference, and polarization drift. Future work, illustrated in Figure 11, will focus on refining the test process and applying near-to-far field conversion models to ensure a more consistent and reliable evaluation of Microstrip Patch Antennas (MPA) designs.

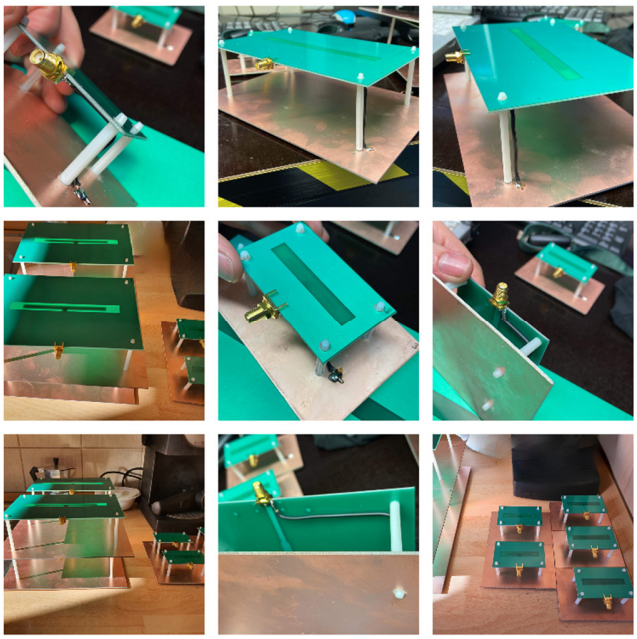

Fig. 11. Future MPA designs for strengthening CPS applications.

ACKNOWLEDGMENT

This research was supported by the University of Debrecen Program for Scientific Publication.

REFERENCES

[1] B. Bordel, R. Alcarria, T. Robles, and D. Martín, "Cyber–physical systems: Extending pervasive sensing from control theory to the Internet of Things," *Pervasive and Mobile Computing*, vol. 40, pp. 156–184, Sep. 2017, https://doi.org/10.1016/j.pmcj.2017.06.011.

[2] G. Zenan, B. Attila, and P. T. Szemes, "Actuator control using TCP IP communication under LabVIEW USB6001 environment," *Carpathian Journal of Electronic and Computer Engineering*, vol. 14, pp. 11-14, Dec. 2021, https://doi.org/10.2478/cjece-2021-0008.

[3] M. Abdel-Wahab and B. and Vogl, "Trends of productivity growth in the construction industry across Europe, US and Japan," *Construction Management and Economics*, vol. 29, no. 6, pp. 635–644, Jun. 2011, https://doi.org/10.1080/01446193.2011.573568.

[4] K. F. Lee and K.-F. Tong, "Microstrip Patch Antennas," in *Handbook of Antenna Technologies*, Springer, Singapore, 2015, pp. 1–55.

[5] C. Peixeiro, "Microstrip patch antennas: An historical perspective of the development," in *2011 SBMO/IEEE MTT-S International Microwave and Optoelectronics Conference (IMOC 2011)*, Natal, Brazil, Jul. 2011, pp. 684–688, https://doi.org/10.1109/IMOC.2011.6169224.

[6] G.A. Deschamps, "Microstrip microwave antennas," in *Proceedings of the Third Symposium on the USAF Antenna Research and Development Program.*, Monticello, IL, USA, 1953, pp. 18–22.

[7] R. Bansal, "Antenna theory; analysis and design," *Proceedings of the IEEE*, vol. 72, no. 7, pp. 989–990, Jul. 1984, https://doi.org/10.1109/PROC.1984.12959.

[8] Kin-Lu Wong, *Planar Antennas for Wireless Communications*, 1st ed. Hoboken, NJ, USA: Wiley, 2003.

[9] B. Chen, Y.-C. Jiao, W. Wang, and F.-S. Zhang, "Modified T-shaped planar monopole antennas for multiband operation," *IEEE Transactions on Microwave Theory and Techniques*, vol. 54, no. 8, pp. 3267–3270, Dec. 2006, https://doi.org/10.1109/TMTT.2006.877811.

[10] C. Kan, Y. Fang, C. J. Anumba, and J. I. Messner, "A cyber–physical system (CPS) for planning and monitoring mobile cranes on construction sites," *Proceedings of the Institution of Civil Engineers - Management, Procurement and Law*, vol. 171, no. 6, pp. 240–250, Dec. 2018, https://doi.org/10.1680/jmapl.17.00042.

[11] N. K. Majji, V. N. Madhavareddy, G. Immadi, and N. Ambati, "A Low-Profile Electrically Small Serrated Rectangular Patch Antenna for RFID Applications," *Engineering, Technology & Applied Science Research*, vol. 14, no. 2, pp. 13611–13616, Apr. 2024, https://doi.org/10.48084/etasr.6989.

[12] V. Akhilesh, "Design and development of microwave patch antennas using conductive polymers," Ph.D. dissertation, Faculty of Engineering, Computer and Mathematical Sciences, The University of Adelaide, Adelaide, Australia, 2011.

[13] V. B. Ramakrishnaiah, R. F. Kubichek, and S. Muknahallipatna, "Mitigation of Terrain Effects using Beamforming Antennas in Ad Hoc Networks," *Discoveries in Agriculture and Food Sciences*, vol. 6, no. 6, pp. 15–15, 2018, https://doi.org/10.14738/tnc.66.5481.

[14] A. Gadda, S. Bedra, C. Agaba, S. Benkouda, R. Bedra, and T. Fortaki, "COMPUTER-AIDED DESIGN OF SUPERCONDUCTING EQUILATERAL TRIANGULAR PATCH ON ANISOTROPIC SUBSTRATES," *Progress In Electromagnetics Research M*, vol. 86, Jan. 2019, Art. no. 203–211, https://doi.org/10.2528/PIERM19090803.

[15] G. Brown, Ed., "60 - A resistive SWR indicator," in *Radio and Electronics Cookbook*, Oxford: Newnes, 2001, pp. 210–212.

[16] A. Abhishek and P. Suraj, "Dual band beam steering antenna using branch line coupler network for higher band applications," *Frequenz*, vol. 79, no. 1–2, pp. 15–28, Jan. 2025, https://doi.org/10.1515/freq-2024-0078.

AUTHOR'S PROFILE

Masuk Abdullah pursued an engineering degree in Mechatronics and Aviation studies and a PG in Strategic Engineering and Sustainability Leadership at the University of Debrecen, Hungary. Since 2023, he has been a faculty member working as a department engineer and course lecturer at the Department of Vehicles Engineering at the University of Debrecen. Masuk is a dedicated professional in IT-ML, mechatronics, strategic engineering, aviation, sustainability, and leadership within engineering management contexts.